INL/CON-21-63795-Revision-0

Pronghorn Porous Media Model Validation with Pressure Drop Measurements

March 2022

Jieun Lee , Stephen King, Yassin A. Hassan, Thien Nguyen , Paolo Balestra, Guillaume Louis Giudicelli, Sebastian Schunert

Changing the World's Energy Future

Idaho National Laboratory

INL is a U.S. Department of Energy National Laboratory operated by Battelle Energy Alliance, LLC

INL/CON-21-63795-Revision-0

Pronghorn Porous Media Model Validation with Pressure Drop Measurements

Jieun Lee , Stephen King, Yassin A. Hassan, Thien Nguyen , Paolo Balestra, Guillaume Louis Giudicelli, Sebastian Schunert

March 2022

Idaho National Laboratory
Idaho Falls, Idaho 83415

http://www.inl.gov

Prepared for the
U.S. Department of Energy
Under DOE Idaho Operations Office
Contract DE-AC07-05ID14517

The 19th International Topical Meeting on Nuclear Reactor Thermal Hydraulics (NURETH-19) Log nr.: 19001
Brussels, Belgium, March 6 - 11, 2022

PRONGHORN POROUS MEDIA MODEL VALIDATION WITH PRESSURE DROP MEASUREMENTS

Jieun Lee, Stephen King, Yassin A. Hassan, Thien Nguyen
Department of Nuclear Engineering
Texas A&M University
AI Engineering Building 3133, 423 Spence St, College Station, TX 77843
jieun.lee@tamu.edu; sdking319@tamu.edu; y-hassan@tamu.edu; thien.duy.ng@tamu.edu

Paolo Balestra, Sebastian Schunert, Guillaume Giudicelli
Idaho National Laboratory
1955 N. Fremont Ave, P.O. Box 1625, Idaho Falls, ID 83415
paolo.balestra@inl.gov; sebastian.schunert@inl.gov; guillaume.giudicelli@inl.gov

ABSTRACT

The verification and validation of Pronghorn is imperative to assert its accuracy when predicting the fluid velocity, temperature, and pressure in high-temperature gas-cooled reactors. Pronghorn is a coarse-mesh, intermediate-fidelity, and multidimensional thermal-hydraulics code developed by the Idaho National Laboratory. The Pronghorn porous media flow model is verified by STAR-CCM+ and validated with new pebble-bed experiments for observing the details of the fluid motion and pressure drop in the porous bed.

This paper focuses on the validation of both the Pronghorn compressible and incompressible Navier-Stokes equations using pressure drop measurements performed at the engineering-scale pebble-bed facility at Texas A&M University. Various pressure drop correlations and porosity functions are implemented in both Pronghorn and STAR-CCM+ to compare the pressure drop due to the combined viscous and inertial resistances in the porous bed. Correlations accounting for the near-wall effect are also utilized to investigate the potential for improvement.

Pronghorn porous media models predict the pressure drop well relative to the STAR-CCM+ simulation results and 1D correlations, and both the finite element method and finite volume method implementations perform similarly. Pronghorn models are also validated with the experimental measurements given different Reynolds number ranges and specific aspect ratios. There exists strong evidence that there is no statistically significant difference in the mean values, such as the pressure drop measurements, specific correlations, or simulations, provided that the overlap of their confidence intervals is more than the half of a single arm. Several validation metrics show similar levels of agreement to other studies. The precise average pebble-bed porosity estimation has a large impact on the pressure drop, and the Foumeny and Montillet (dense packing) models provide an accurate pressure drop prediction while also considering the near-wall effect.

KEYWORDS
Porous media modeling, verification and validation, high-temperature gas-cooled reactors, pebble-bed reactors, Navier-Stokes equations

1. INTRODUCTION

The verification and validation of Pronghorn is critical for building confidence in the prediction of the fluid behavior in advanced reactors, specifically high-temperature gas-cooled reactors (HTGRs). The HTGR is

an advanced Generation IV reactor concept and can produce the process heat for industrial applications along with electricity generation [1, 2] and inherent safety features, such as the passive decay heat removal [3, 4].

Pronghorn is a coarse-mesh, intermediate-fidelity, and multidimensional thermal-hydraulics (TH) code developed by Idaho National Laboratory [5–7]. It allows for the modeling of multidimensional phenomena and reduces the computational cost by homogenizing small-scale features. Figure 1 describes the hierarchy of TH modeling and its characteristics. Furthermore, Pronghorn is flexible in coupling Idaho National Laboratory Multiphysics Object-Oriented Simulation Environment based simulation tools, such as RELAP-7 for the system safety analysis, BISON for the fuel performance, and Griffin for the neutronics applications.

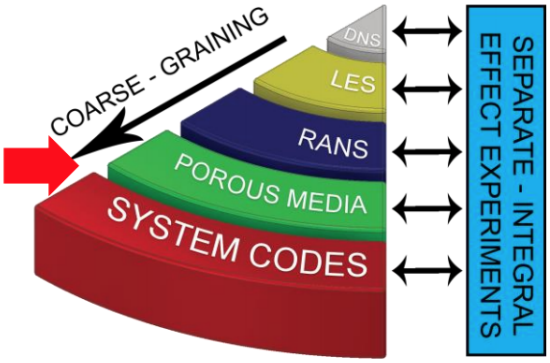

Figure 1. Hierarchy of TH modeling [5].

Extensive studies related to correlations (of the porosity, pressure drop, effective thermal conductivities, and solid-fluid convective heat transfer coefficient) for porous beds have been performed [8–11]. However, the validation of the correlations applicable for HTGRs in the porous media models (herein, Pronghorn) is still necessary because the flow condition in HTGRs is different from other porous media applications. The high fluid flow rates are expected in pebble-bed reactors (PBRs), and the aspect ratio, defined as the bed diameter divided by the pebble diameter, is relatively high.

This motivates the Pronghorn verification and validation with Texas A&M University (TAMU) isothermal versatile experiments [12], provided that the preliminary results [13] show an excellent agreement of Pronghorn porous media flow models with STAR-CCM+ for the solid and fluid temperatures in the SANA pebble-bed experiments. This includes the implementation of correlations applicable to the pebble-bed experiments in Pronghorn, the comparison of the pressure drop correlations with those simulated by STAR-CCM+, and the studies related to the interaction of the near-wall and bulk flows in the PBRs (in other words, the near-wall effect). Here, pressure drop measurements under the isothermal condition are compared with simulation results from both Pronghorn and STAR-CCM+ Navier-Stokes/Darcy-Forchheimer models given the average pebble-bed porosity and pressure drop correlations.

2. THEORY

2.1. Governing Equations

The macroscale modeling approach is established to predict the mass, momentum, and heat transfer phenomena in porous media. The continuum concept is applied by taking an average of properties within the representative elementary volume [14, 15]. However, the model still requires knowledge of the closures for estimating the effective properties based on the pore-scale characteristics knowledge. Therefore, the Darcy-Forchheimer model is used with the Navier-Stokes equations at the continuum scale [16].

The compressible Navier-Stokes equations are used to account for the conservation of fluid mass and momentum [11]. The fluid continuity equation is given by

$$\varepsilon \frac{\partial \rho_f}{\partial t} + \nabla \cdot (\varepsilon \rho_f u) = 0 \, , \tag{1}$$

where ρ_f is the fluid density, t is the time, u is the interstitial/physical velocity, and ε is the porosity, which is the fluid volume divided by the total volume. The conservation of momentum equation for the fluid is

$$\varepsilon \frac{\partial (\rho_f u)}{\partial t} + \nabla \cdot (\varepsilon \rho_f u u) + \varepsilon \nabla P - \varepsilon \rho_f g + W \rho_f u - \nabla \cdot (\varepsilon \mu \nabla u) = 0 \, , \tag{2}$$

where P is the pressure, g is the gravitational acceleration vector, W is the interphase friction factor, and μ is the dynamic viscosity.

The thermal equilibrium porous media model from the third-party computational fluid dynamics software, STAR-CCM+, uses the same formulation as the Pronghorn compressible Navier-Stokes equations [17]. Note that the constant density model is applied in both Pronghorn and STAR-CCM+ for water since it is only slightly compressible.

2.2. Average Pebble-Bed Porosity/Drag Coefficients

The average porosity, $\bar{\varepsilon}$, of a randomly packed bed of pebbles varies depending on the packing method and aspect ratio, and it can be approximated by utilizing correlations derived from experimental measurements [11]. Table I contains a summary of the correlations selected to calculate the average porosity. Note that the aspect ratio is defined as the ratio of the bed diameter, D, over pebble diameter, d_p. The average porosity is commonly used to develop the following pressure drop correlations in porous media in Table II.

The empirical correlations are used to predict the pressure drop (ΔP) of the fluid due to pebbles in the reactor. Generally, the friction factor varies depending on the pebble diameter, porosity, and fluid properties, such as the fluid density and dynamic viscosity. Some correlations use the aspect ratio to consider the near-wall effect, and others use the tortuosity to introduce the effect of the transverse flow. Table II introduces three major pressure drop correlations and their validity conditions used in Pronghorn and STAR-CCM+ simulations, and other correlations are described in [11].

Table I. Average porosity correlations

Author	Validity Condition	Ave. Porosity Correlation	Bed Diameter (mm)	Pebble Diameter (mm)	Material for Spheres/Packing Method	Material for the Column
Mueller [18]	$\frac{D}{d_p} \geq 2.02$	$0.365 + 0.22\frac{d_p}{D}$ $\pm\, 0.0055/D$ (SD propagated)	25.75, 50.50, 76.00, 101.88	12.751	Clear Lucite plexiglass/random packing	Clear cast acrylic cylindrical container
Sato et al. [19]	$\frac{d_p}{D} < 0.4$	$0.3517 + 0.4657\frac{d_p}{D}$ $\pm\, 0.0076$ (max. SD of measurements)	65.8, 122	2.59, 12.2, 24.3	Glass spheres/gently dumped	Acrylic tubes
Zou and Yu (loose, dense packing) [20]	$\frac{d_p}{D} \leq 0.256$	$0.4+0.01(e^{10.686\frac{d_p}{D}}-1)$	35, 54, 62, 74, 90, 104, 127, 172, and 194	1, 2, ..., 12 (glass beads) 15.8, 25.8, and 37.0 (marble balls)	Glass beads and marble balls/random packing	—
	$\frac{d_p}{D} \leq 0.253$	$0.372+$ $0.002(e^{15.306\frac{d_p}{D}}-1)$				

SD is the standard deviation.

The particle Reynolds number is defined as

$$Re_p = \frac{\rho_f u_s d_p}{\mu} \,, \tag{3}$$

where u_s is the superficial velocity. The superficial velocity is calculated by

$$u_s = \varepsilon u \,. \tag{4}$$

The modified Re number (Re^*) is obtained by dividing the particle Reynolds number by $1-\varepsilon$.

$$Re^* = \frac{\rho_f u_s d_p}{\mu(1-\varepsilon)} \tag{5}$$

In Table II, H is the length of the porous medium, and the average porosity is used to calculate the superficial velocity, modified Re number, and pressure drop in the porous bed.

2.3. Equations of State

The TAMU isothermal versatile experiments have either air or water going through the porous bed. Either the ideal gas law or constant density model is applied to calculate the fluid density. The fluid properties are obtained from [24–26].

2.4. Mesh Convergence Study

The spatial convergence study is critical in estimating the discretization error in computational fluid dynamics simulations [27–29]. When numerical (coarse, medium, and fine mesh) solutions are in the asymptotic range, and their higher-order terms are small (in other words, the observed order of accuracy, $\hat{p}$,

Table II. Pressure drop correlations

Author	Pressure Drop Correlation	Validity Condition		
		Porosity Range	Aspect Ratio Range	Re^* or Re_p Range
Ergun [21]	$\Delta P = \left[150\mu\frac{(1-\bar{\varepsilon})^2}{\bar{\varepsilon}^3}\frac{u_s}{d_p^2} + 1.75\rho_f\frac{(1-\bar{\varepsilon})}{\bar{\varepsilon}^3}\frac{u_s^2}{d_p}\right] H,$ $f_{Ergun} = \frac{150}{Re^*} + 1.75$	$0.36 < \bar{\varepsilon} < 0.65$	$\frac{D}{d_p} > 10$	$1 < Re^* < 2500$
Eisfeld and Schnitzlein [22]	$\Delta P = \left[154A_w^2\mu\frac{(1-\bar{\varepsilon})^2}{\bar{\varepsilon}^3}\frac{u_s}{d_p^2} + \frac{A_w}{B_w}\rho_f\frac{(1-\bar{\varepsilon})}{\bar{\varepsilon}^3}\frac{u_s^2}{d_p}\right] H,$ where $A_w = 1 + \frac{2}{3(D/d_p)(1-\bar{\varepsilon})}$ and $B_w = \left[1.15\left(\frac{d_p}{D}\right)^2 + 0.87\right]^2,$ $f_{Eisfeld} = \frac{154A_w^2(1-\bar{\varepsilon})^2}{Re_p\bar{\varepsilon}^3} + \frac{A_w(1-\bar{\varepsilon})}{B_w\bar{\varepsilon}^3}$	$0.33 \leq \bar{\varepsilon} \leq 0.882$	$1.624 \leq \frac{D}{d_p} \leq 250$	$0.01 \leq Re_p \leq 17,635$
KTA [23]	$\left[160\mu\frac{(1-\bar{\varepsilon})^2}{\bar{\varepsilon}^3}\frac{u_s}{d_p^2} + 3(\frac{1-\bar{\varepsilon}}{Re_p})^{0.1}\rho_f\frac{(1-\bar{\varepsilon})}{\bar{\varepsilon}^3}\frac{u_s^2}{d_p}\right] H,$ $f_{KTA} = \frac{320}{Re^*} + \frac{6}{Re^{*0.1}}$	$0.36 < \bar{\varepsilon} < 0.42$	$\frac{D}{d_p}$ above the limiting curve in [23], $H > 5d_p$	$1 < Re^* < 10^5$

Here, f is the friction factor.

is close to the formal order of accuracy, $\bar{p}$, of the discretization scheme), the Richardson extrapolation can be used to predict the quantity for a mesh with an infinite number of elements [29].

The GCI describes the discretization error compared to the asymptotic numerical value in a percentage, and it is to ensure a 95% confidence level for the computed value [28, 29]. The two GCIs are calculated by Eq. 6 given the constant refinement ratio for three different mesh refinement levels.

$$GCI_{21} = F_s\frac{|e_{21}|}{r^p - 1} \text{ and } GCI_{32} = F_s\frac{|e_{32}|}{r^p - 1}\ , \tag{6}$$

where F_s is the safety factor and e_{21} and e_{32} are the relative errors defined by

$$e_{21} = \frac{f_2 - f_1}{f_1}, \text{ and } e_{32} = \frac{f_3 - f_2}{f_2}\ . \tag{7}$$

Here, r is the refinement ratio, and f_1, f_2, and f_3 are the quantities of interest estimated for the fine, medium, and coarse mesh. The value of p is determined by Table III. The uncertainty estimate can be obtained by taking the absolute value of the discretization error [29]. Finally, by satisfying the relation between two GCIs in Eq. 8, the solutions from all three mesh refinement levels are in the asymptotic range of convergence [27].

$$GCI_{32} = r^p GCI_{21} \tag{8}$$

Table III. Implementation of the GCI method [29]

Condition	p	F_s
$\lvert\frac{\hat{p}-\bar{p}}{\bar{p}}\rvert \leq 0.1$	$\bar{p}$	1.25
$\lvert\frac{\hat{p}-\bar{p}}{\bar{p}}\rvert > 0.1$	$\min(\max(0.5, \hat{p}), \bar{p})$	3.0

3. GEOMETRY & MESH SETUP

The TAMU pebble-bed test facility design is shown in Figure 2. The experiments estimated the behavior of the gas flow in the pebble bed, although they assumed an isothermal condition. Two different pebble sizes provide the aspect ratios of 11 and 7.33 to observe the near-wall effect of PBRs. One compressible fluid (air) and one incompressible fluid (water) were used to measure the pressure drop within the designated porous bed heights. Table IV describes the detailed geometric configuration of the TAMU pebble-bed test facility and specifies the experimental conditions. Note that the same size of pebble bed was used for both the incompressible and compressible cases, a bed diameter of 0.1397 m. The experiments cover the flow range from the laminar to turbulent regime for validating the correlations. In other words, the particle Reynolds number varies from 55 to 678.

In Figure 3, for the axisymmetric model, the uniform mesh with 1,024 cells is used for the free flow region where only the pure fluid is provided, and 12,800 and 14,080 elements are used in the porous region with air and water. For the STAR-CCM+ and Pronghorn finite volume (FV) cases, the boundary conditions are the inlet velocity, outlet pressure, and free-slip conditions on the walls. The initial conditions are the ambient temperature and pressure. For the Pronghorn finite element (FE) cases, the Dirichlet boundary conditions are used for the inlet velocities. The implicit boundary condition (i.e., a boundary condition that uses the correct velocity specified for the momentum equation) for the advective term in the mass equation is also specified at both the outlet and inlet in FE simulations. In addition, the implicit boundary for the advection term in the momentum equation is determined at the outlet, and the outlet pressure is weakly imposed for the pressure term in the momentum equation.

Table IV. Geometric configuration of the TAMU pebble-bed test facility and its experimental conditions

Experimental Conditions	
Working fluid	Air, water
Working fluid temperature (^{o}C)	21, 25
Material for the pebbles and cylindrical bed	Acrylic
Bed diameter (m)	0.1397
Pebble diameter (m)	0.0127, 0.01905
Bed height (m)	1.219, 1.2954
Aspect ratio (bed diameter/pebble diameter)	11, 7.33

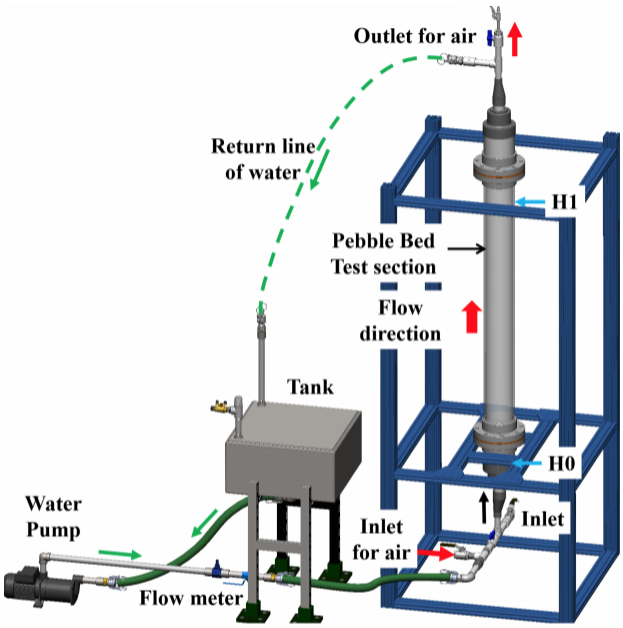

Figure 2. Schematic of the pebble bed test facility from [12].

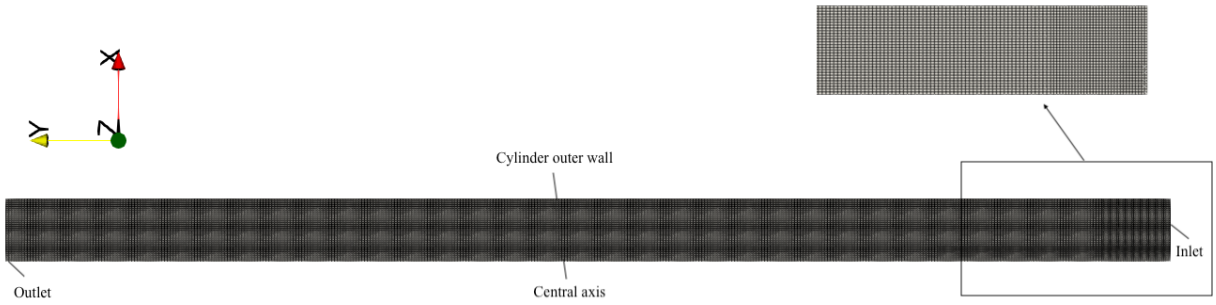

Figure 3. Geometry and fine mesh of the Pronghorn and STAR-CCM+ models (axisymmetric modeling).

4. SIMULATION SETTINGS/NUMERICAL METHODS

Pronghorn with the finite element method (FEM) uses the Streamline Upwind Petrov-Galerkin method to discretize the Navier-Stokes equations. The details of the weak form of compressible Navier-Stokes equations implemented in Pronghorn are provided in [11]. The Newton method is used to solve the system of coupled nonlinear equations, and Pronghorn reaches a steady-state solution by running a pseudo-transient simulation. In addition, Pronghorn can also run FV simulations, and the preliminary pressure drop results are presented in this study. Here, the first-order upwind scheme is used for advection, and the fully coupled solver is used.

The finite volume method is used by STAR-CCM+ v16.02.009. STAR-CCM+ generates the reference solutions for quantities, such as the pressure drop and velocity profile, and the steady state solutions under the laminar/turbulent flow condition are obtained with the Darcy-Forchheimer model. The second-order

upwind scheme is used for convection, and the segregated SIMPLE solver is used.

5. RESULTS & DISCUSSION

The average porosity of a randomly packed bed was estimated by the correlations. We investigated twelve different average porosity correlations from [11]. Mueller, Sato, and Zou and Yu correlations were selected because their experimental setups are similar to the TAMU isothermal experiments, and the parameters of the TAMU experiments fall within the correlations' validity conditions. These correlations were developed by the researchers with pebble and bed diameters similar to the current experiments, including the random packing method and the pebble material, such as acrylic glass. On the other hand, we excluded other correlations derived from experiments different from the TAMU experiments. For instance, Beavers et al. [30] derived the correlation by using a rectangular bed, and Foumeny et al. [31] vibrated the cylinder to pack the pebbles. In Figure 4, *red* lines represent the aspect ratios of 11 and 7.33 used for the air and water cases, respectively. The uncertainty bands are provided for the Mueller and Sato correlations by propagating the SDs of the pebble diameter. The uncertainties are calculated by multiplying the SDs by 2 for the 95% confidence level given the normal distributions, and they are less than 1% of the average porosities at the corresponding aspect ratios of 11 and 7.33. Note that the Zou model is considered with both the loose and dense packing methods. The average porosities calculated by the above correlations vary within the porosity range by ∼0.05, which is relatively large compared to the values of the averages. This would likely provide the differences in pressure drop when the empirical pressure drop correlations are applied in the Darcy-Forchheimer model (see Table V).

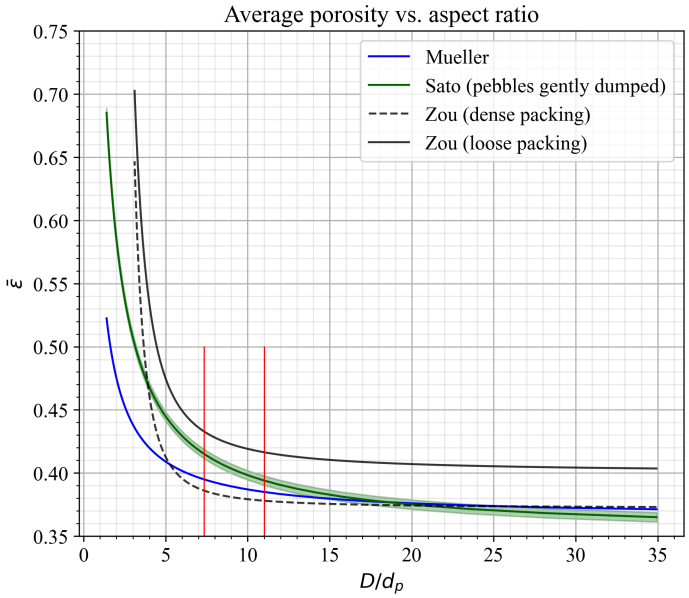

Figure 4. Comparison of average porosity correlations.

The optimal porosity function was determined by examining the porosity functions in Table V; these functions were used with the pressure drop correlations listed in Table VI to produce Figure 5. As a result, the Zou average porosity function with dense packing estimates the pressure drop better than others, specifically for air cases. Given that both the experimental and correlation data are deterministic, the Zou

Table V. Average porosities estimated by different correlations

Model/Average Porosity	$\bar{\varepsilon}$ (air)	$\bar{\varepsilon}$ (water)
Mueller	0.385	0.395
Sato (pebbles gently dumped)	0.394	0.4152
Zou (dense packing)	**0.378**	0.3861
Zou (loose packing)	0.4164	**0.4329**

model with dense packing has the lowest root mean square errors (RMSEs), relative root mean square errors (RRMSEs), and average Euclidean distances (commonly known as L^2 norm). The probabilistic experimental data led to the same conclusion such that the Zou dense packing model performs the best in predicting the pressure drop with the lowest averages of the total normalized Euclidean distance with the Eisfeld and Schnitzlein and KTA correlations (see Table VI). On the other hand, the Zou loose packing model approximates the pressure drop better than other models for the water cases with regard to the validation metrics in Table VII. The equations for the validation metrics are described in detail in [32].

Table VI. Validation metrics for the Zou dense packing model (air)

Validation Metrics/Model (1D calculation)	Ergun	Eisfeld and Schnitzlein	KTA
Average relative difference (%)	8.496	12.76	13.19
RMSE (Pa)	12.04	43.07	26.53
RRMSE (%)	5.488	19.63	12.09
L^2 norm (Pa)	34.06	121.8	75.04
Average of the total normalized Euclidean distance	2.966	4.56	4

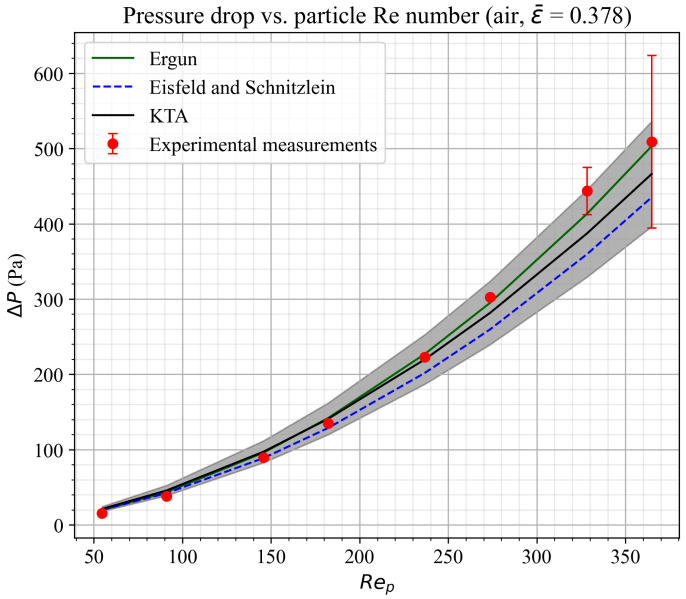

Figure 5. Pressure drop comparison with the Zou dense packing model (air).

The specification of the turbulence quantities did not improve the pressure drop significantly. The turbulent quantities are specified for the pebble-bed region for $Re_p = 274 \sim 365$ (see Figure 7 for the Foumeny function), and the SST $k-\omega$ model with the all y+ wall treatment is used for the free flow region with no slip condition. Due to the insignificant pressure drop change by applying the turbulence quantities to the compressible Navier-Stokes equations with the Darcy-Forchheimer model, the axisymmetric model is utilized without the turbulence properties for the whole Reynolds number range for both Pronghorn and STAR-CCM+.

Table VII. Validation metrics for the Zou loose packing model (water)

Validation Metrics/Model (1D calculation)	Eisfeld and Schnitzlein	KTA
Average relative difference (%)	37.61	39.82
RMSE (Pa)	52.04	51.17
RRMSE (%)	18.89	18.58
L^2 norm (Pa)	194.7	191.5
Average of the total normalized Euclidean distance	0.7963	0.7833

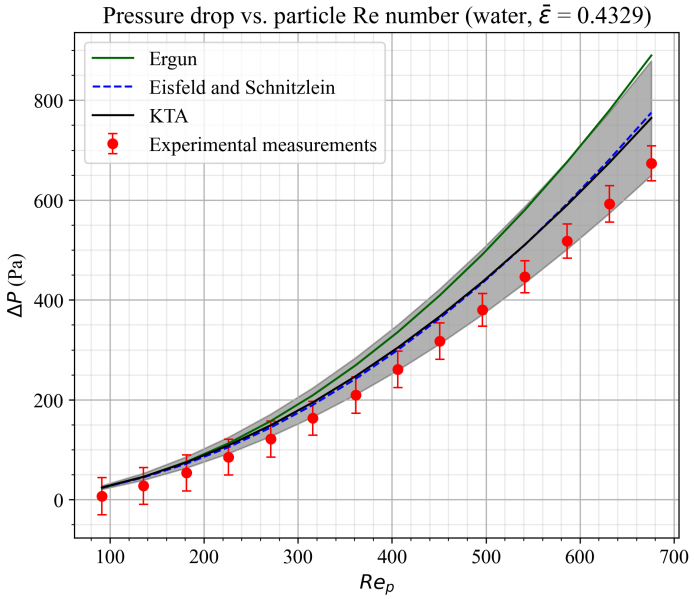

Figure 6. Pressure drop comparison with the Zou loose packing model (water).

After determining the average porosity, numerous pressure drop correlations valid in the specific Reynolds number and aspect ratio ranges were implemented in both Pronghorn and STAR-CCM+ to estimate the pressure drop in the pebble bed. First, the mesh convergence test was performed such that the results are spatially converged. Generally, the GCIs for fine meshes are less than 1% with the lowest and highest particle Reynolds numbers for air and water; therefore, the uncertainty error bars are estimated as a conservative error of 1% of the predicted pressure drop. Peculiarly, they are evaluated as 1.5% of the pressure drop as approximated by the STAR-CCM+ with the Foumeny function given the turbulence

quantities in the porous region. This shows that the fine meshes, in general, provide numerical results close to the asymptotic solutions with the uncertainty errors less 1% and ensure a higher than 99% confidence level for the computed values.

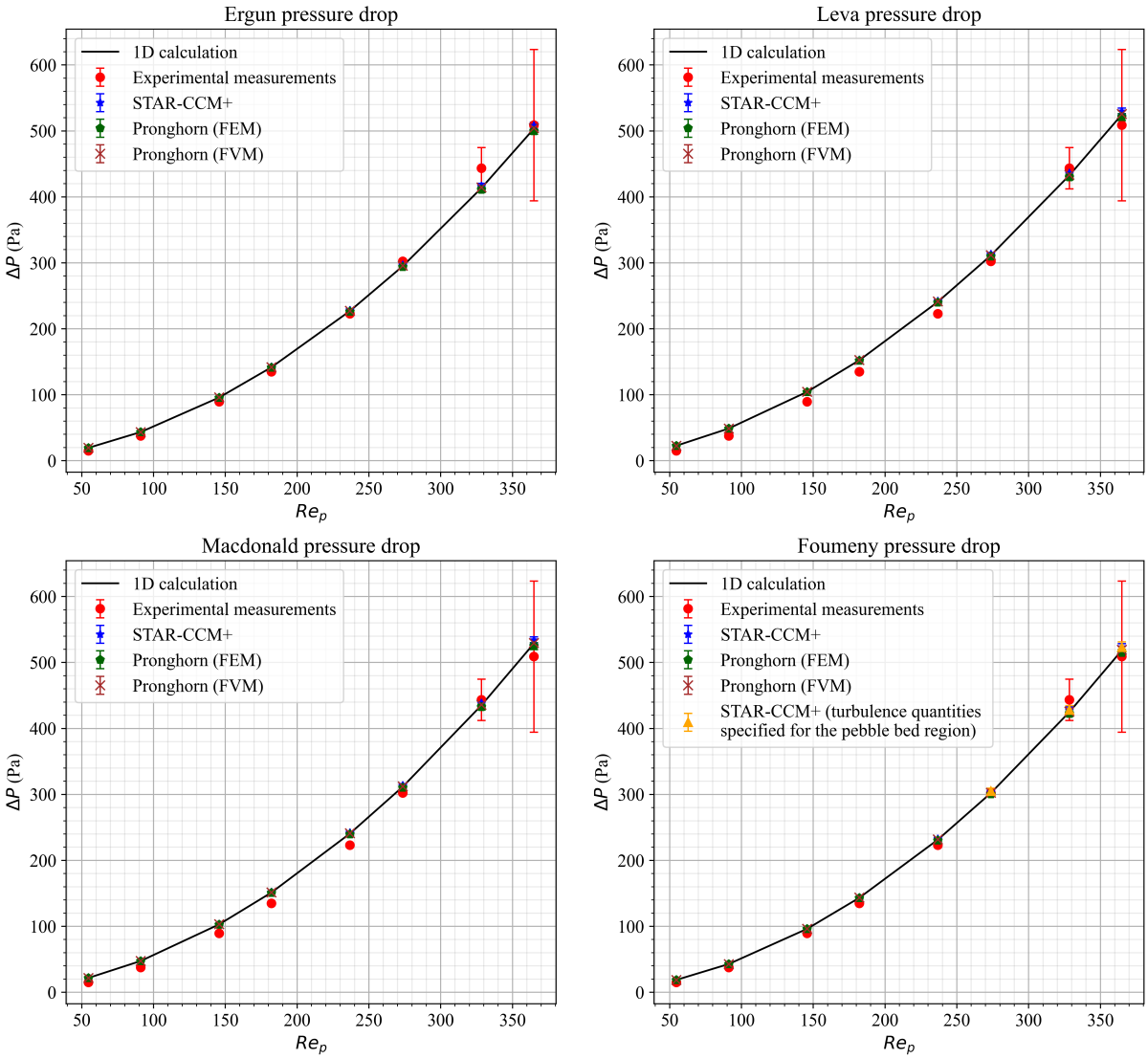

Figure 7. Pressure drop correlations for air.

In Figure 7, although the Ergun correlation is developed with the substantially small pebble and bed diameters, and pebbles are packed with vibration, it estimates the experimental pressure drop data fairly well with an average relative difference of 8.5% for both the 1D calculation and Pronghorn (FE) compared to the experiments and with an 8.34% average relative difference for the STAR-CCM+ results. Macdonald et al. used much smaller particles; however, the similar packing material and method may result in pressure drop measurements within the 50% prediction band from [33]. The Foumeny function, which considers the aspect ratio in calculating the pressure drop, predicts the pressure drop the most accurately among other valid correlations in [11] (see Table VIII); however, the Cheng, Eisfeld and Schnitzlein, Harrison, and Liu

functions, which also use the bed diameter to account for the near-wall effect, deteriorate the pressure drop calculation. Figure 8 describes the gauge pressure and velocity magnitude profiles of the Re_p = 365 case given the Foumeny function. Not only do the simulation results from Pronghorn and STARCCM+ agree well, but they comparably estimate the experimental pressure drop.

For the experiments with the nearly incompressible fluid (water), the Montillet dense packing model results in the lowest RMSEs, RRMSEs, L^2 norms, and averages of the total normalized Euclidean distance with Pronghorn and STAR-CCM+. The Montillet function was developed based on the similar pebble and bed sizes, including the random packing of glass particles, and it considers the near-wall effect to improve the pressure drop prediction. Here, the aspect ratio of 7.33 is small such that the near-wall effect is probably influential. Although the average relative differences in Table VIII are beyond the maximum relative difference of 10.4% in [34], in Figure 9, overall, the overlap of the 95% confidence interval bars of the experiments and simulation results is more than the half of a single arm. Therefore, the two-tailed p-value is $\leq$0.05, and it provides strong evidence for the null hypothesis of the zero difference in means [35–37]. In other words, the statistical significant effect is most likely small.

Table VIII. Validation metrics for the Foumeny and Montillet functions (for air and water)

Validation Metrics/Model	Foumeny			Montillet (dense packing)		
	Pronghorn (FE)	Pronghorn (FV)	STAR-CCM+	Pronghorn (FE)	Pronghorn (FV)	STAR-CCM+
Average relative difference (%)	7.454	7.707	7.779	26.69[§]	27.37[§]	26.92[§]
RMSE (Pa)	9.2754	9.161	9.355	10.9	12.19	11.23
RMSRE	0.1032	0.1055	0.105	0.6687[*]	0.6742[*]	0.6715[*]
RRMSE (%)	4.227	4.175	4.264	3.958	4.424	4.075
L^2 norm (Pa)	26.23	25.91	26.46	40.79	45.59	42
Average of the total normalized Euclidean distance	2.902	3.082[†]	3.094[‡]	0.1621	0.1821	0.1671

[†]The Ergun function provides a similar average of the total normalized Euclidean distance of 3.028 by Pronghorn (FV) for air.
[‡]The Ergun function provides a similar average of the total normalized Euclidean distance of 3.012 by STAR-CCM+ for air.
[§]The Meyer function brings similar average relative differences of 24.21, 24.16, and 24.26 for Pronghorn (FE), Pronghorn (FV), and STAR-CCM+, respectively.
[*]The Meyer function shows similar RMSREs of 0.6298, 0.6347, and 0.6324 for Pronghorn (FE), Pronghorn (FV), and STAR-CCM+, respectively.

6. CONCLUSIONS AND FUTURE WORK

The Pronghorn (both the FEM and FVM) pressure drop prediction agrees well with the STAR-CCM+ simulation results and 1D correlations, including the experimental pressure drop measurements given the different Reynolds number ranges and specific aspect ratios. The precise prediction of the porosity function

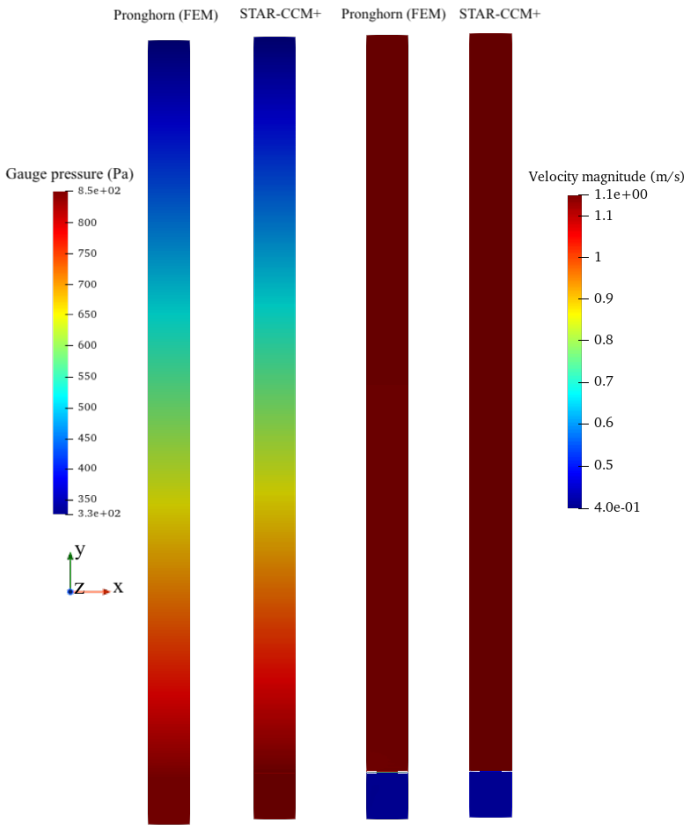

Figure 8. Gauge pressure and velocity magnitude profiles estimated by the Foumeny function with Pronghorn and STAR-CCM+ for Re_p = 365.

has an impact on the pressure drop results, and by considering the near-wall effect, the Fomeny and Montillet models perform the most accurately for air and water, accordingly.

The studies related to the velocity profile estimation are in process by considering the radial (oscillatory/exponential) porosity functions. Further research about the impact of the turbulence quantities in the porous region on the velocity, influence of utilizing the volume-averaged porosity in the arbitrary volumes, and transport of the high-fidelity data into the porous media models are recommended. Additionally, the validation metrics with the experimental and model probabilistic data may be obtained by determining the robust simulation uncertainty.

ACKNOWLEDGMENTS

This research was partially funded by the Office of Nuclear Energy of the U.S. Department of Energy, NEAMS project, under Contract No. DE-NE0008983. This research made use of the resources of the High Performance Computing Center at Idaho National Laboratory, which is supported by the Office of Nuclear Energy of the U.S. Department of Energy and the Nuclear Science User Facilities under Contract No. DE-AC07-05ID14517.

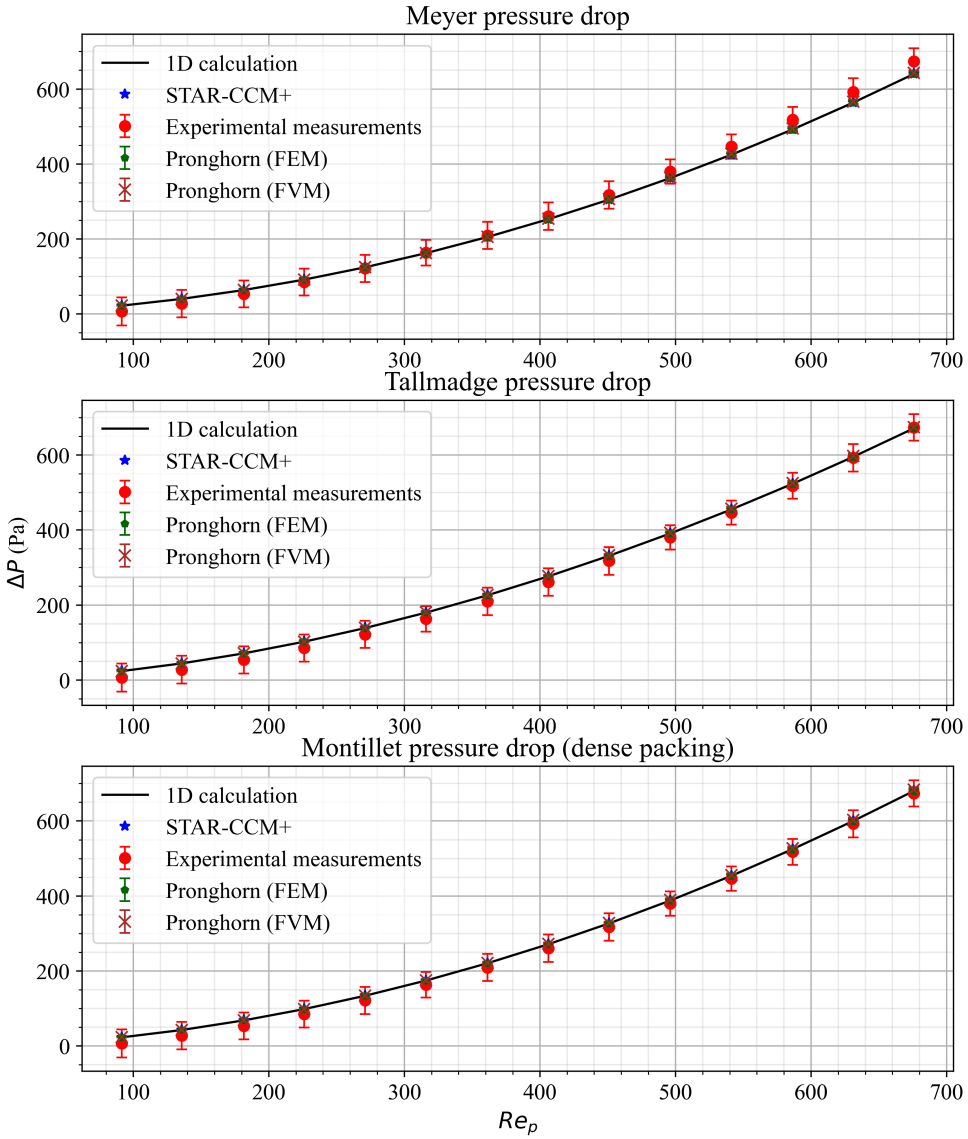

Figure 9. Pressure drop correlations for water.

REFERENCES

1. I. Pioro and R. Duffey, "Current and Future Nuclear Power Reactors and Plants," in *Managing Global Warming*, pp. 117–197, Academic Press, https://doi.org/10.1016/B978-0-12-814104-5.00004-1 (2019).

2. J. Beck and L. Pincock, "High Temperature Gas-Cooled Reactors Lessons Learned Applicable to the Next Generation Nuclear Plant," INL/EXT-10-19329, Idaho National Laboratory, Idaho Falls, ID, USA, https://doi.org/10.2172/1023461 (2011).

3. T. Wilson Jr, S. Ball, R. Wood, M. Cetiner, and W. Poore, "Advanced Control and Protection System Design Methods for Modular HTGRs," ORNL/TM-2012/170, Oak Ridge National Laboratory, Oak Ridge, TN, USA, https://doi.org/10.2172/1047629 (2012).

4. H. Reutler and G. Lohnert, "Advantages of Going Modular in HTRs," *Nuclear Engineering and Design*, **78** (2), pp. 129–136, https://doi.org/10.1016/0029-5493(84)90298-X (1984).

5. Pronghorn Development and Analysis Group, "Pronghorn: a Coarse Mesh Thermal-Hydraulics Application Based on MOOSE for Advanced Reactor Concepts," NUC Workshop - Innovations in Advanced Reactor Design, Analysis, and Licensing, Raleigh, NC, USA (2019).

6. A. Novak et al., "Multiscale Thermal-Hydraulic Modeling of the Pebble Bed Fluoride-Salt-Cooled High-Temperature Reactor," *Annals of Nuclear Energy*, **154**, pp. 107968, https://doi.org/10.1016/j.anucene.2020.107968 (2021).

7. A. Novak et al., "Pronghorn: a Multidimensional Coarse-Mesh Application for Advanced Reactor Thermal Hydraulics," *Nuclear Technology*, **207** (7), pp. 1–32, https://doi.org/10.1080/00295450.2020.1825307 (2021).

8. Y. Hassan and C. Kang, "Pressure Drop in a Pebble Bed Reactor under High Reynolds Number," *Nuclear Technology*, **180** (2), pp. 159–173, https://doi.org/10.13182/NT12-A14631 (2012).

9. E. Erdim, Ö. Akgiray, and İ. Demir, "A Revisit of Pressure Drop-Flow Rate Correlations for Packed Beds of Spheres," *Powder Technology*, **283**, pp. 488–504, https://doi.org/10.1016/j.powtec.2015.06.017 (2015).

10. Z. Guo, Z. Sun, N. Zhang, and M. Ding, "Influence of Confining Wall on Pressure Drop and Particle-to-Fluid Heat Transfer in Packed Beds with Small D/d Ratios under High Reynolds Number," *Chemical Engineering Science*, **209**, pp. 115200, https://doi.org/10.1016/j.ces.2019.115200 (2019).

11. A. Novak et al., "Pronghorn Theory Manual," Idaho National Laboratory, Idaho Falls, ID, USA (2021).

12. S. King et al., "Pressure Drop Measurements in a Versatile Experimental Facility of Packed Spheres," *American Nuclear Society*, **117** (1), pp. 1713–1716 (2017).

13. J. Lee et al., "Pronghorn Fully Compressible Equation Set Validation Against SANA Open Plenum Experiments," *Proc. HTR*, Virtual Conference, June 2–5 (2021).

14. M. Quintard, "Introduction to Heat and Mass Transport in Porous Media," STO-EN-AVT-261, Von Karman Institute for Fluid Dynamics, Rhode Saint Genese, Belgium (2015).

15. J. Bear, *Dynamics of Fluids in Porous Media*, Courier Corporation (2013).

16. D. Takhanov, "Forchheimer Model for Non-Darcy Flow in Porous Media and Fractures," Imperial College London, London, United Kingdom (2011).

17. "CFD/CCM User Guide Version 2020.1," Siemens (2020).

18. G. Mueller, "Radial Void Fraction Distributions in Randomly Packed Fixed Beds of Uniformly Sized Spheres in Cylindrical Containers," *Powder Technology*, **72** (3), pp. 269–275, https://doi.org/10.1016/0032-5910(92)80045-X (1992).

19. Y. Sato, T. Hirose, F. Takahashi, and M. Toda, "Pressure Loss and Liquid Holdup in Packed Bed Reactor with Cocurrent Gas-Liquid Down Flow," *Journal of Chemical Engineering of Japan*, **6** (2), pp. 147–152, https://doi.org/10.1252/jcej.6.147 (1973).

20. R. Zou and A. Yu, "The Packing of Spheres in a Cylindrical Container: the Thickness Effect," *Chemical Engineering Science*, **50** (9), pp. 1504–1507, https://doi.org/10.1016/0009-2509(94)00483-8 (1995).

21. S. Ergun, "Fluid Flow through Packed Columns," *Chem. Eng. Prog.*, **48**, pp. 89–94 (1952).

22. B. Eisfeld and K. Schnitzlein, "The Influence of Confining Walls on the Pressure Drop in Packed Beds," *Chemical Engineering Science*, **56** (14), pp. 4321–4329, https://doi.org/10.1016/S0009-2509(00)00533-9 (2001).

23. Geschäftsstelle des Kerntechnischen Ausschusses, "KTA, Reactor Core Design of High-Temperature Gas-Cooled Reactors. Part 3: Loss of Pressure through Friction in Pebble Bed Cores," 3102.3, Nuclear Safety Standards Commission, Berlin, Germany (1981).

24. E. Lemmon, R. Jacobsen, S. Penoncello, and D. Friend, "Thermodynamic Properties of Air and Mixtures of Nitrogen, Argon, and Oxygen from 60 to 2000 K at Pressures to 2000 MPa," *Journal of Physical and Chemical Reference Data*, **29** (3), pp. 331–385, https://doi.org/10.1063/1.1285884 (2000).

25. R. Montgomery, "Viscosity and Thermal Conductivity of Air and Diffusivity of Water Vapor in Air," *Journal of Atmospheric Sciences*, **4** (6), pp. 193–196, https://doi.org/10.1175/1520-0469(1947)004<0193:VATCOA>2.0.CO;2 (1947).

26. C. J. R. and R. B. Dooley, "Release on the IAPWS Formulation 2008 for the Viscosity of Ordinary Water Substance," IAPWS R12-08, International Association for the Properties of Water and Steam, Berlin, Germany (2008).

27. L. Kwaśniewski, "Application of Grid Convergence Index in FE Computation," *Bulletin of the Polish Academy of Sciences*, **61** (1), pp. 123–128 (2013).

28. L. Schwer, "Is Your Mesh Refined Enough? Estimating Discretization Error Using GCI," *7th LS-DYNA Anwenderforum*, **1** (1), pp. 45–54 (2008).

29. W. Oberkampf and C. Roy, *Verification and Validation in Scientific Computing*, Cambridge University Press (2010).

30. G. Beavers, E. Sparrow, and D. Rodenz, "Influence of Bed Size on the Flow Characteristics and Porosity of Randomly Packed Beds of Spheres," *Journal of Applied Mechanics*, **40** (3), pp. 655–660, https://doi.org/10.1115/1.3423067 (1973).

31. E. Foumeny, F. Benyahia, J. Castro, H. Moallemi, and S. Roshani, "Correlations of Pressure Drop in Packed Beds Taking into Account the Effect of Confining Wall," *International Journal of Heat and Mass Transfer*, **36** (2), pp. 536–540, https://doi.org/10.1016/0017-9310(93)80028-S (1993).

32. K. A. Maupin, L. P. Swiler, and N. W. Porter, "Validation Metrics for Deterministic and Probabilistic Data," *Journal of Verification, Validation and Uncertainty Quantification*, **3** (3), pp. 031002, https://doi.org/10.1115/1.4042443 (2018).

33. I. Macdonald, M. El-Sayed, K. Mow, and F. Dullien, "Flow through Porous Media-the Ergun Equation Revisited," *Industrial & Engineering Chemistry Fundamentals*, **18** (3), pp. 199–208, https://doi.org/10.1021/i160071a001 (1979).

34. A. Montillet, E. Akkari, and J. Comiti, "About a Correlating Equation for Predicting Pressure Drops through Packed Beds of Spheres in a Large Range of Reynolds Numbers," *Chemical Engineering and Processing: Process Intensification*, **46** (4), pp. 329–333, https://doi.org/10.1016/j.cep.2006.07.002 (2007).

35. G. Cumming, F. Fidler, and D. Vaux, "Error Bars in Experimental Biology," *Journal of Cell Biology*, **177** (1), pp. 7–11, https://doi.org/10.1083/jcb.200611141 (2007).

36. G. Cumming, "Inference by Eye: Reading the Overlap of Independent Confidence Intervals," *Statistics in Medicine*, **28** (2), pp. 205–220, https://doi.org/10.1002/sim.3471 (2009).

37. D. Lane et al., *Introduction to Statistics*, Citeseer (2017).